IEEE Access
Multidisciplinary ⋮ Rapid Review ⋮ Open Access Journal

Received October 23, 2020, accepted November 3, 2020. Date of publication xxxx 00, 0000, date of current version xxxx 00, 0000.

Digital Object Identifier 10.1109/ACCESS.2020.3036548

Intelligent Optimization Strategy Based on Statistical Machine Learning for Spacecraft Thermal Design

YAN XIONG[1,2], LIANG GUO[1], DEFU TIAN[1,2], YANG ZHANG[1,2], AND CHUNLONG LIU[1]

[1]Department of Space Robot Engineering, Changchun Institute of Optics, Fine Mechanics and Physics, Chinese Academy of Sciences, Changchun 130033, China
[2]University of Chinese Academy of Sciences, Beijing 100049, China

Corresponding author: Liang Guo (guoliang@ciomp.ac.cn)

The work received funding from the National Natural Science Foundation of China (Grant No. 61605203) and the Youth Innovation Promotion Association of Chinese Academy of Sciences (Grant No. 2015173).

ABSTRACT The thermal design of spacecraft becomes increasingly complicated as various advanced technologies are continuously introduced to the spacecraft. Determining and optimizing the uncertainties of a spacecraft thermal control system through global sensitivity analysis has long been an essential task for thermal engineers. It is a difficult task that relies heavily on engineering experience and is a time-intensive, trial-and-error endeavor that may not even lead to global optimization. Hence, an intelligent optimization strategy based on statistical machine learning for spacecraft thermal design, called IOSML, is proposed. An intelligent batch processing system (IBPS) based on MATLAB, Python, and NX/TMG real-time data interaction is designed. The IBPS uses a surrogate model to reduce the computational cost of global sensitivity analysis while using a detailed thermal mathematical model to maintain accuracy. We combine a Bayesian inference framework with a neural network surrogate spacecraft-thermophysical model that is 100× faster than numerical solvers. This article first reports on a density-based global sensitivity analysis that evaluates the effect of design parameters on the temperature difference between the complementary metal–oxide–semiconductor and cold screen of the Lehman Alpha Solar Space Telescope detector. From 42 design parameters, the most sensitive four are selected for optimization, and the temperature difference and the boundary temperature are used as the objective function. Adopting IOSML, under no supervision, four design parameters are optimized through the IBPS, and the effectiveness of the algorithm is verified by comparison with traditional methods. Additionally, IOSML is versatile and can be used in various complex engineering applications to provide guidance for the better selection of appropriate parameters and optimization.

INDEX TERMS Global sensitivity analysis, spacecraft thermal design, machine learning, optimization.

I. INTRODUCTION

Temperature is a major factor affecting the performance of space telescopes [1]. The uniformity of the space temperature and the control of the rate of the temperature change critically affect the quality of space telescope imaging. Thermal design is particularly important to the temperature control of space telescopes, as many parameters of the thermal design affect performance. The optimization of thermal design is thus essential for the accurate and stable imaging of space telescopes [2]–[4]. Typically, black-box optimization methods (adopting, for example, experimental design, a genetic algorithm [5]–[8], a particle swarm algorithm [9], or the non-dominated sorting genetic algorithm II [10]) are used in the optimization of thermal design. Selected variables are systematically modified within a certain range and the response surface of the system is mapped [11], [12] to reach an optimal design. These methods have great potential for the thermal design of spacecraft, are highly cost effective, and are generally speculated to be the ideal choice for the thermal design parameter optimization of spacecraft to be developed for future deep-space exploration. However, the conventional black-box optimization approach has limitations in that the thermal design engineer's choice of variables and their range artificially limits the parameter space and the maximum performance improvement that can be achieved. Furthermore,

The associate editor coordinating the review of this manuscript and approving it for publication was Weipeng Jing.

insights into the root causes of poor performance have been severely limited.

Optimization of the spacecraft thermal design first requires a global sensitivity analysis (GSA) [13], [14] to define uncertainties in the spacecraft thermal control system. This requires many space thermal analyses to be performed to achieve appropriate thermal control. These analyses are time-consuming finite element analyses [15]–[17] that solve partial differential equations. Several meta-modeling approaches that replace the original model with approximate or surrogate models can be adopted to improve the computational efficiency. These approaches include support vector regression [18] and the use of artificial neural networks and have been adopted in the optimization of the thermal design of spacecraft. However, these methodologies require a detailed thermal mathematical model (DTMM) [19]–[21] to guarantee adequate accuracy of the metamodel and are time consuming to employ [22], [23]. Stout [24] proposed a Bayesian-based thermal modeling approach to optimize the thermal design of spacecraft, but the computational efficiency of their approach struggles to satisfy engineering requirements.

Conversely, Bayesian optimization [25]–[27] has recently been combined with physics-based forward models. Fast, simple, and temperature-dependent current–voltage measurements allow the statistically rigorous optimization of the thermal control of early stages of spacecraft, providing new insight for further improvements in methods of optimizing the thermal design of spacecraft. In the present paper, an intelligent optimization strategy based on statistical machine learning for spacecraft thermal design, called IOSML, is proposed to improve on traditional methods of optimizing the thermal design of spacecraft [28], [29]. This is the first time that Bayesian optimization algorithms have been applied to the optimization of spacecraft thermal design. Additionally, IOSML differs from traditional methods of optimizing spacecraft thermal design that adopt time-consuming Monte Carlo estimation. IOSML involves an intelligent batch processing system based on MATLAB, Python, and NX/TMG [30] real-time data interaction (IBPS), whereby the cost of GSA is reduced using a surrogate model [31] while a DTMM is used to maintain accuracy. The system automatically evaluates the model within its variation space according to sampling inputs without supervision, and it is at least 5 times faster than traditional artificial Monte Carlo estimation. In particular, we combine the Bayesian inference framework with a neural network surrogate model [32]. This is a novel approach based on the hybrid strategy of using artificial neural networks in approximating nonlinear systems, which has been applied to approximate the computation of spacecraft thermophysical models and is 10 times faster than a numerical solver. The present paper first evaluates the effect of a temperature difference between the complementary metal–oxide–semiconductor (CMOS) and the cold screen of the SCI121.6 detector (TD_CS) onboard the Lehman Alpha Solar Space Telescope (LST) via a density-based GSA of the thermal design parameters. From 42 thermal design parameters, four parameters are selected as optimization parameters, and the TD_CS and boundary temperature are then employed to construct the target function. The automatic optimization of the optimization parameters is performed without supervision via the IBPS using IOSML.

The remainder of the paper is organized as follows. Section II presents the background and motivation of the study. Section III presents details of the IOSML design methodology. Section IV presents the application of IOSML to the optimization of the thermal design parameters of the LST, and compares the performance of IOSML with that of three classical optimization methods. Finally, conclusions of the study are presented in Section V.

II. BACKGROUND AND MOTIVATION

A. SURROGATE MODEL

Surrogate models are used in engineering when quantities of interest are not easily and directly measurable [33]. This approach has the potential to speed up complex modeling without sacrificing accuracy or detail and can reduce numerical instability, thereby facilitating calibration and uncertainty analysis.

A growing number of scholars are investigating surrogate models. We typically group agent modeling techniques into three categories: data-driven, projection, and hierarchy-based approaches [34]. In particular, the data-driven surrogate model approximates the thermophysical model via an empirical model that captures the original model's input–output mapping. Projection-based models reduce the dimensionality of the parameter space by projecting governing equations onto the basis of a normal vector. Conversely, hierarchical or multi-fidelity methods create surrogate models by simplifying the physical system; e.g., by ignoring certain processes or by reducing the accuracy of numerical calculations.

In this article, we propose a novel surrogate model approach by combining the advantages of the above three types of surrogate model to improve the efficiency of thermal design optimization and to guarantee the accuracy of thermal analysis.

B. BAYESIAN OPTIMIZATION

Bayesian optimization is a powerful strategy for discovering the optimal value of an objective function that has high evaluation costs [35], [36]. It is applicable in cases that one does not have a closed-form expression of the objective function but can make observations of that function at the sampled value.

In general, Bayesian optimization is a typical example of model-based sequential optimization [37]–[40]. The Bayesian optimization framework has two components: a Bayesian surrogate model for modelling the objective function and an acquisition function for deciding where to sample next. The surrogate models are frequently in the form of Gaussian Processes (GPs) [41], which provide efficient representations of complex functions and characterize model

uncertainty in probabilistic frameworks, consequently also called a probabilistic surrogate model. The search for the optimum is guided by an acquisition function that is defined on the statistical surrogate and defines a metric for evaluating the next point to sample through a continuous trade-off between a global exploration and a local exploitation of the surrogate.

Initial sampling strategies are often an important consideration in sequential model-based optimization. Available approaches mainly include random, quasi-random, and Latin hypercube sampling (LHS) of the domain [42].

Specifically, we consider the problem of finding the maximum value of an expensive function $f : A \to \mathbb{R}$,

$$x^{opt} = \arg\max_{x \in A} f(x). \tag{1}$$

where the input x is in $\mathbb{R}^d$ for a value of d that is typically small. It is noted that $d \leq 20$ in most cases of the successful application of Bayesian optimization. The feasible set A is a simple set for which it is easy to evaluate membership.

We consider a dataset of n paired input/output observations $D_n = \{(x_i, y(x_i))\}_{i=1}^n$, with $x_i \in \mathbb{R}^d$ and $y(x_i) \in \mathbb{R}$, generated by the unknown mapping function $y(x) = f(x) + \varepsilon$, where $\varepsilon \sim N(\mu_\varepsilon, \sigma_\varepsilon)$. GP regression defines a supervised problem in which we associate to the function f a GP prior having mean function m and covariance function $\kappa : \mathbb{R}^d \to \mathbb{R}$,

$$f(x) \sim GP(m(x), \kappa(x, x')). \tag{2}$$

We denote the kernel matrix by $K \in \mathbb{R}^{n \times n}$, such that $K(i, j) = \kappa(x_i, x_j)$. $\kappa_n(x) \doteq (\kappa(x, x_1), \ldots, \kappa(x, x_n))$, the predictive distribution of the GP, is defined by the mean function $\mu(x)$ and the variance function $\sigma(x)$:

$$\mu(x) = \kappa_n(x)^T (K + \sigma_\varepsilon I)^{-1} y \tag{3}$$

$$\sigma^2(x) = \kappa(x, x) - \kappa_n(n)^T (K + \sigma_\varepsilon I)^{-1} \kappa_n(x) \tag{4}$$

where $y \doteq (y(x_1), \ldots, y(x_n))^T$ denotes the set of hyperparameters and I is the n-dimensional identity matrix.

Once we have a statistical model that reflects our beliefs about the unknown function f given D_n, we need a sampling strategy or policy to select new query points x_{n+1}. Available approaches mainly include random sampling, quasi-random sampling, and LHS of the domain. In this article, we adopt a novel LHS-optimized strategy proposed by Huntington and Lyrintzis [43]. The acquisition function used in this article is the expected improvement, which can be evaluated analytically:

$$\begin{aligned} EI(x) &= E\left[\max\left(f(x) - f\left(x^+\right), 0\right)\right] \\ &= \begin{cases} \left(\mu(x) - f\left(x^+\right) - \zeta\right)\Phi(Z) + \sigma(x)\phi(Z) & \text{if } \sigma(x) > 0 \\ 0 & \text{if } \sigma(x) = 0 \end{cases} \end{aligned} \tag{5}$$

where $\phi(\cdot)$ and $\Phi(\cdot)$ are respectively the probability density function and cumulative distribution function of a standard normal distribution. $f(x^+)$ denotes the maximum value and x^+ is the corresponding sample location. μ is the mean of all observations while σ is the standard deviation of all observations. $EI(\cdot)$ seeks the expectation that the unknown point function value is greater than $f(x^+)$, while Z the standardized improvement

$$Z = \begin{cases} \dfrac{(\mu(x) - f(x^+) - \zeta))}{\sigma(x)} & \text{if } \sigma(x) > 0 \\ 0 & \text{if } \sigma(x) = 0 \end{cases} \tag{6}$$

where the parameter ζ allows adjustment of the tradeoff between exploration and exploitation, determining the relative importance of the posterior mean $\mu(x)$ versus the potential improvement in the region with high uncertainty; i.e., large $\sigma(x)$.

III. INTELLIGENT OPTIMIZATION STRATEGY

This section presents an intelligent optimization strategy based on statistical machine learning. A method of surrogate modelling based on the artificial neural network is first introduced. Important parameters are then obtained through GSA of the thermal design parameters. Next, the setting of the objective function and other important parameters required for Bayesian optimization according to the optimization goal are presented. Finally, the practical workflow of IOSML is presented in detail.

A. INTELLIGENT BATCH PROCESSING SYSTEM FOR THE THERMAL ANALYSIS OF A SPACE TELESCOPE

Thermophysical models of space telescopes have many parameters, and traditional methods of spacecraft thermal control require thermal engineers to manually import these parameters into thermal analysis software. In finding the best solution for the thermal design of space telescopes, thermal engineers need to obtain and analyze a large amount of data from thermal analysis results for different modeling parameters. This requires much repetitive work and is time consuming and error prone. An intelligent batch system for thermal analysis based on machine learning is therefore proposed in this article. The system automatically creates a sample input space and conducts batch thermal analysis and the extraction of generated data without supervision. This reduces the effort and time required and improves the efficiency of thermal analysis.

The IBPS has multiple functional modules, such as modules for the sampling of the thermal design parameters, the loading of parameters, and the extraction of results of space thermal analysis (see Fig. 1). Additionally, the IBPS realizes the unsupervised automatic construction of datasets of the space thermal analysis results, which effectively reduces the effort and time required and improves the efficiency of space thermal analysis.

B. REPLACEMENT OF THE THERMOPHYSICAL MODEL WITH A SURROGATE MODEL

Thermal radiation is the main mode of heat transfer in the thermal analysis of spacecraft, and Monte Carlo ray tracing [44] is the method most widely adopted in the analysis of

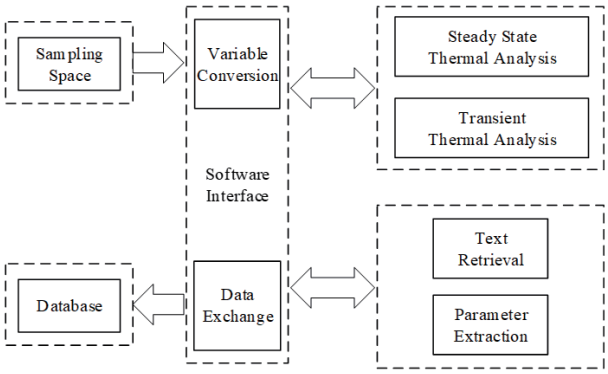

FIGURE 1. Workflow of the batch processing system.

thermal radiation. However, Monte Carlo ray tracing has an extremely long calculation time and requires a great computational resource; i.e., it demands exceptionally high performance of a computer's graphics card. Therefore, to improve the efficiency of thermal analysis, a simplified model (surrogate model) of the spacecraft thermal analysis model must be constructed without reducing the overall computational accuracy.

There are also many methods for formulating surrogate models, such as the Response Surface Method (RSM) [45], Radical basic function (RBF) [46], Support Vector Regression (SVR) [47], Kriging [48], Sparse Polynomial Chaos Expansions (SPCE) [49], etc…RSM is one of the widely available surrogate models. For problems with N input variables, there are $\frac{(N+1)(N+2)}{2}$ coefficients required to be determined; the third-order and higher-order models are intolerable with an increase in the number of variables. In general, RSM is only applicable to the approximation of low nonlinear models. RBF does not require the specification of an objective function expression or derivative information, which requires only the selection of a radial basis function to efficiently construct a relatively accurate surrogate model with a small amount of input data. The support vector machine [50] is one of the most widely used machine learning algorithms for applying kernel tricks to solve pattern recognition problems and was first introduced by Cortes and Vapnik [51]. And it was extended to a nonlinear regression based on the support vector machine framework, called SVR. However, when solving the models with large sample sets, high input dimensions, and strong nonlinearities, the SVR must spend a significant amount of computational time solving the quadratic planning which is the core process of the SVR [52]. The Kriging model has high approximation accuracy for various nonlinear functions, which has been widely used in the field of optimization. However, the construction of the Kriging model is too slow and there are some problems such as premature convergence for certain objective functions with a wide range of response values. SPCE is a popular surrogate modeling approach, which exploits polynomial chaos expansion [53], the sparse effects principle, and a powerful sparse regression solver to approximate a nonlinear model with many input parameters, while relying on very little model evaluation. However, as the number of model inputs M increases, the number of polynomials in the expansion will grow rapidly, and the number of samples must be larger than the number of polynomials to guarantee accuracy, so an excessive number of input parameters will cause dimensional catastrophe problems.

On the other hand, heuristic intelligent optimization algorithms, such as genetic algorithms (GA) [54] and particle swarm optimization (PSO) [55] algorithms, have gradually become a research hotspot in recent years. This provides new ideas and means for solving complex problems. The combination of artificial neural networks and heuristic optimization algorithms can significantly improve the accuracy of models. Although classical evolutionary algorithms such as GA and PSO have been successfully applied in various fields with outstanding achievements, their shortcomings cannot be ignored [56]. For example, they cannot utilize feedback from the network in a timely manner, resulting in a slow algorithmic search speed. Additional training time is required to obtain more accurate solutions, and the potential advantages of the algorithm's parallel mechanism is underutilized. In order to overcome the shortcomings of GA and PSO, the Mind Evolution Algorithm (MEA) was first proposed by Sun in 1998 [57], which was inspired by the activity of human mind. Compared with GA and PSO, the MEA converges much faster. After several rounds of comprehensive comparative analysis of the above various methods, the RBF neural network (RBF NN) surrogate model based on the improved mind evolution algorithm is employed in this article to develop the surrogate model of the thermophysical model of the spacecraft, called RBF-IMEA [58]. Here, the RBF is a Gaussian function, for which the activation function is

$$r\left(x_q - c_i\right) = \exp(-\frac{1}{2{\sigma_r}^2}\left\|x_q - c_i\right\|^2) \tag{7}$$

and the output of the network is

$$y_j = \sum_{i=1}^{k} \omega_{ij} \cdot \exp(-\frac{1}{2{\sigma_r}^2}\left\|x_q - c_i\right\|^2), \quad j = 1, 2, \cdots, n \tag{8}$$

where x_q represents the q^{th} input vector of the n dimensional vector x, c_i is the center of the Gaussian function, and ω_{ij} is the weight of connection between the hidden and input layers.

The proposed RBF-IMEA (Fig. 2) includes the following optimization steps:

Step 1: According to the topology of the RBF NN, mapping from the decoding space to the coding space is implemented, and the length of the IMEA code is

$$L = L_1L_2 + L_2L_2 + L_2L_3 + L_2 + L_3 \tag{9}$$

where L_1, L_2, and L_3 are respectively the number of nodes in the input, hidden, and output layers.

Step 2: The reciprocal of the mean squared error of the training set is chosen as the reward function F for each

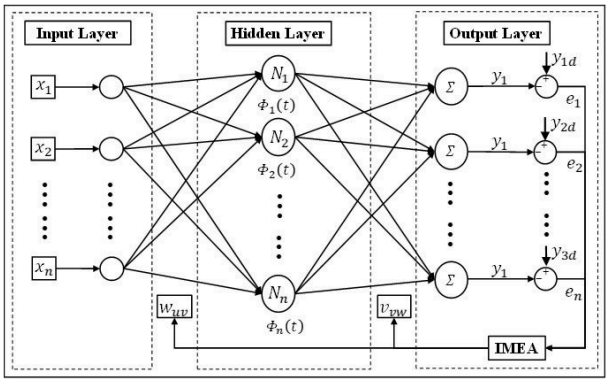

FIGURE 2. Structure of the RBF NN based on the IMEA.

individual and group and expressed as

$$F = \frac{n}{\sum_{i=1}^{n} \left(x_{ok,i} - x_{pre,i}\right)^2} \tag{10}$$

where $x_{obs,i}$ is the true value of the i^{th} sample and $x_{pre,i}$ the predicted value of the i^{th} sample.

Step 3: Initialize the group to obtain an excellent subgroup and a temporary subgroup. After convergence and mutation operations are performed, the global optimal individual and its score are obtained.

Step 4: The optimized parameters obtained from the IMEA are input into the RBF NN for further training.

C. DENSITY-BASED GSA OF THERMAL DESIGN PARAMETERS FOR THE LST

Variance-based GSA methods are widely employed in the thermal design of spacecraft and are usually calculated adopting Monte Carlo estimation. However, such estimation requires many samples to ensure sufficient accuracy, and when modeling is difficult, these analyses are costly to perform and the convergence of GSA is slow. Therefore, an intelligent density-based GSA method based on RBF-IMEA neural networks is proposed. This method adopts a DTMM to maintain accuracy and then adopts an RBF-IMEA neural network trained with data from thermal analysis results under many different thermal modeling parameters to reduce the cost of GSA, which contributes to a more comprehensive understanding of the impact of all model parameters on model performance and can greatly speed up thermal design optimization of spacecraft.

Density-based GSA has long been studied by many authors [59], [60] and gives consideration to the probability distribution of the output rather than just the output at a particular moment in time. Specifically, the sensitivity to x_i is determined by the distance measured between the unconditional probability distribution of y obtained when all inputs change at the same time and the conditional distribution obtained when all inputs except x_i change.

For simplicity, we describe the conditional and unconditional probability distributions in terms of the cumulative distribution function rather than probability distribution functions, as the cumulative distribution function is easier to compute. A time-independent GSA is defined as

$$\delta_i = \frac{1}{2} E_{X_i}\left[s\left(X_i\right)\right] \tag{11}$$

Suppose that $F_Y(y)$ and $F_{Y|X_i}(y)$ intersect at m points, where $y = a_1, a_2, \ldots, a_m$. If $F_Y(a) - F_{Y|X_i}(a_1) > 0$, then

$$s\left(X_i\right) = 2\left\{\begin{array}{l}\left[F_Y\left(a_1\right) - F_{Y|X_i}\left(a_1\right)\right] \\ -\left[F_Y\left(a_2\right) - F_{Y|X_i}\left(a_2\right)\right] + \cdots \\ +(-1)^{(m-1)}\left[F_Y\left(a_m\right) - F_{Y|X_i}\left(a_m\right)\right]\end{array}\right\} \tag{12}$$

If $F_Y(a_1) - F_{Y|Xi}(a) < 0$, then

$$s\left(X_i\right) = 2\left\{\begin{array}{l}\left[F_{Y|X_i}\left(a_1\right) - F_Y\left(a_1\right)\right] \\ -\left[F_{Y|X_i}\left(a_2\right) - F_Y\left(a_2\right)\right] + \cdots \\ +(-1)^{(m-1)}\left[F_{Y|X_i}\left(a_m\right) - F_Y\left(a_m\right)\right]\end{array}\right\} \tag{13}$$

$$E_{Xi}\left[s\left(X_i\right)\right] = \int F_{X_i}\left(x_i\right) s\left(X_i\right) dx_i \tag{14}$$

Here, δ_i is the sensitivity index of input X_i to Y, $s(X_i)$ the separation of the output density $F_Y(y)$ and the conditional density of Y, $F_{Y|X_i}(y)$ given X_i, and $F_{X_i}(x_i)$ is the density of X_i. The expectation $E_{X_i}[s(X_i)]$ accounts for the average shift in the decision-maker's view of the output provoked by Xi.

D. PRACTICAL WORKFLOW OF IOSML

IOSML proposed in this article has three phases and six steps. Full use is made of three programming languages and space thermal analysis software (Fig. 3).

Stage 1: A thermophysical model of the spacecraft is first established using the node network method (NNM) [61]. Sampling in the range of thermal modeling parameters is then conducted to create a sample input space based on the LHS method, which is imported by the IBPS into the DTMM for batch space thermal analysis to maintain the accuracy of the model output in an unsupervised manner. The spacecraft thermophysical model computed by the IBPS is then approximated using the RBF-IMEA neural network as a function of the tracking GSA, while the surrogate model based on a neural network can greatly accelerate post-processing. Finally, convergence analysis is conducted to evaluate the fitting performance of the RBF-IMEA neural network and to decide whether to extend the sampling space further.

Stage 2: An LHS-based sampling space is first generated for the GSA. Density-based GSA is then performed for the thermal modeling parameters, and the effect of each thermal modeling parameter on the telescope CMOS temperature and TD_CS is evaluated according to the GSA results. Here RBF-IMEA neural network surrogate model is adopted in the GSA process instead of the space thermal analysis model to accelerate the thermal analysis. Several groups of key parameters are selected for post-optimization according to the degree of influence.

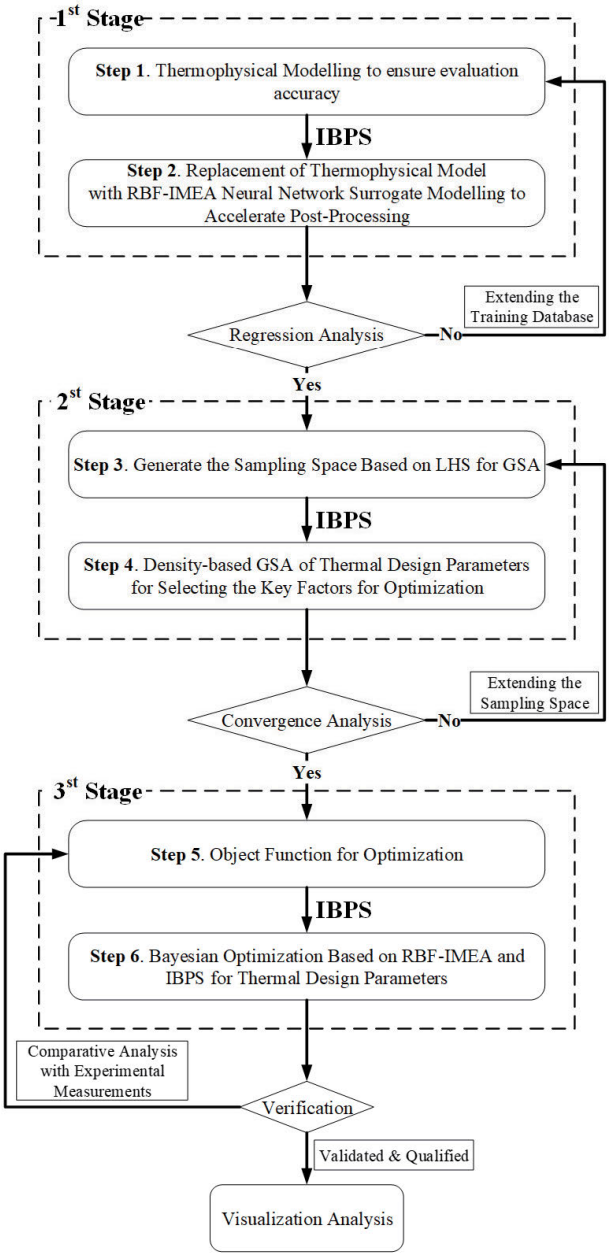

FIGURE 3. Practical workflow of IOSML.

Stage 3: The optimal objective function is first determined according to thermal control requirements. The thermal design parameters of the space telescope are then optimized by the Bayesian optimization algorithm through the IBPS without supervision.

IV. EXAMPLE APPLICATIONS AND RESULTS

To verify its performance, IOSML was applied to the optimization of the thermal design parameters of the Extreme Ultraviolet (EUV) detector of the space-based LST, which was designed and manufactured in China, and its performance compared with that of a genetic algorithm (GA), particle swarm optimization algorithm (PSO), and Powell algorithm (POW) [62]–[65].

This section describes the application of IOSML to the LST in depth. The background of the LST is first provided. A thermophysical model of the LST is then described. Furthermore, intelligent optimization of the thermal design parameters of the LST under high-temperature conditions is carried out using IOSML proposed in this article. Finally, the performance of IOSML is compared with that of the GA, PSO, and POW.

A. BACKGROUND OF THE LST

To allow astronomers to observe and study various solar activities, such as coronal mass ejections, solar flares, and sunspots, the Chinese Academy of Sciences designed a novel space-based Lyman alpha and visible dual-band internally buried coronagraph that satisfies the requirements of simultaneous high-resolution imaging and observation of the corona at wavelengths of 121.6 and 700 nm. The overall structure of the LST is shown in Fig. 4A. The barrel of the primary mirror permanently faces the sun. The SCI 121.6 detector and SCI 700 detector are two core detectors of the LST and are essential for observing and studying the internal activity and dynamics of the solar interior in the 121.6-nm and 700-nm bands. The parameters and settings of the orbital environment are given in Table 1, showing that the LST operates in a solar-synchronous orbit at an altitude of 720 km and is exposed to a complex thermal environment, including direct sunlight, infrared radiation from the Earth, and sunlight reflected from the Earth (see Fig. 5). Additionally, there is a large difference in heat flux between the sunny side and shaded side, which may result in an uneven temperature distribution between the primary mirror and detector, thus affecting the imaging quality of the LST. Consequently, there is a strong desire to design a reliable, efficient, and accurate thermal control system for the LST, especially for the detector.

TABLE 1. Parameters and settings of the orbital environment.

Parameter	Hot case	Cold case
Orbit	Sun-synchronized orbit	
Minimum Altitude	$720km$	
Spacecraft Attitude	Lens barrel is facing the sun and orbiting under inertia	
Satellite Position	Local Time at Ascending Node 18:00:00	
Orbit Period	$5942.6s$	
Orbit Inclination	$98.38°$	
Albedo	0.306	
CMOS Power	$0.65W$	
System Heating Power	$\leq 120W$	
Temperature Index for Frameworks	19∼25°C	
Stefan-Boltzmann Constant	$5.67\times10^{-8}W/(\mathrm{m}^2\cdot K^4)$	
Solar Constant	$1412W/m^2$	$1322W/m^2$
Earth IR	$237W/m^2$	$220W/m^2$

The LST requires a high level of precision in thermal control both during storage and operation owing to the complexity and variability of the space environment. The working temperature of the frame ranges from 19 to 25°C. The operating temperature of the SCI121.6 detector must

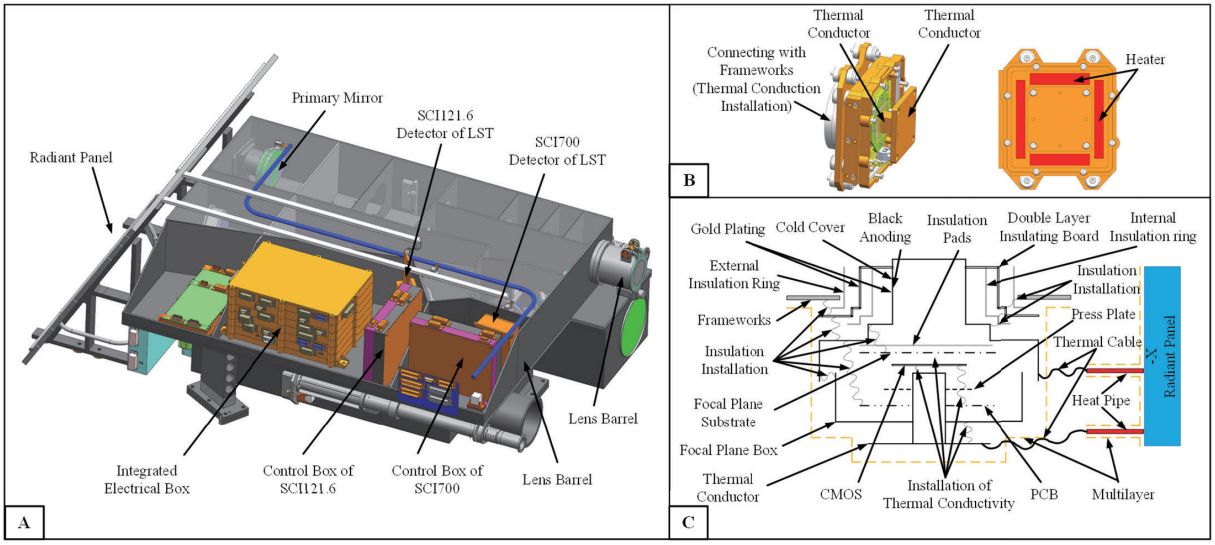

FIGURE 4. Overall structure of the LST and detector. (A) Overall structure of the LST. (B) Heaters attached to the SCI121.6 detector. (C) Structural diagram of the SCI121.6 detector.

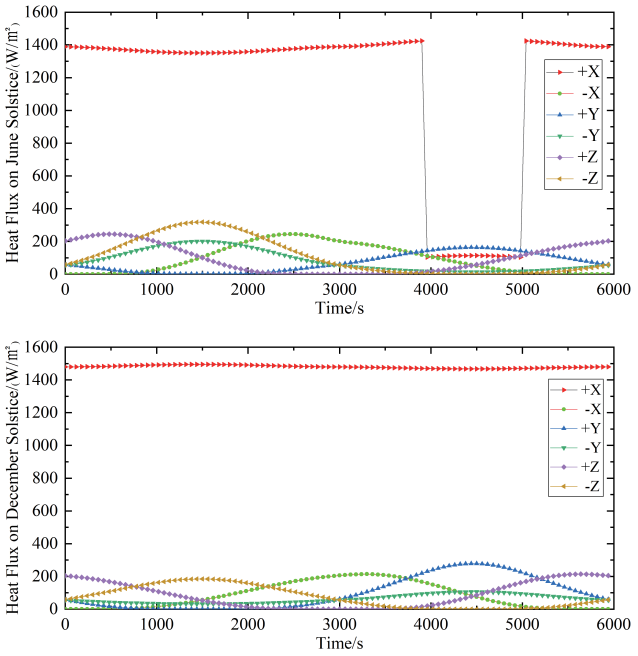

FIGURE 5. External heat flux of the LST in hot and cold cases.

be maintained between 50 and 20°C. The CMOS within the SCI121.6 detector has aluminum ammonia heat pipes for cooling (see Fig. 4C) but the pipes will fail when their temperature falls below 70°C, and it is thus essential to control the temperature of the CMOS in the range of 30 to 25°C, which poses a great challenge in the thermal design of the SCI121.6 detector. Figure 4B illustrates the structure of the well-designed SCI 121.6 detector. The cold plate utilizes electron convection generated by the temperature difference between the cold plate and CMOS to achieve a controlled flow of micro-dust and other pollutants to decontaminate and ensure the imaging quality of the CMOS. This requires that the temperature of the cold plate be lower than that of the CMOS, and the temperature difference (TD_CS) should be maintained above 5°C. Table 2 specifies the materials used in the detector and their physical properties, which are affected by manufacturing and processing (see Table 3). In particular, in terms of ensuring the accuracy of temperature control of important components such as the CMOS and heat pipes and ensuring that the temperature difference between the CMOS and cold plate is always greater than 5°C, relying on the experience of thermal design engineers would be time consuming and make it almost impossible to optimize a large number of thermal design parameters.

TABLE 2. Materials used in the detector and their physical properties.

Name	Material	Density	Thermal conductivity	Specific heat capacity
Focal plane box	Aluminum alloy (2A12)	2780	121	921
CMOS	Photosensitive material	1800	20	500
PCB	Composite materials	1800	20	500
Thermal conductor	Aluminum alloy (7A09)	2850	134	921
Thermal cable	Copper	8750	350	400
Cold cover	Aluminum alloy (7A09)	2850	134	921
Insulation pads/rings	Polyimide	1420	0.25	1130

TABLE 3. Surface processes and their thermophysical properties.

Name	Solar absorptivity	Infrared emissivity
Black anodizing	0.80-0.95	0.80-0.95
Gold plating	0.15-0.40	0.02-0.05
S781 white coatings	0.12-0.25	0.80-0.94
F46	0.11-0.45	0.60-0.80

Bayesian optimization is a powerful strategy for obtaining optimal values of objective functions with high evaluation costs. To validate its performance in the optimization of

the thermal design of space telescopes, IOSML is applied to the optimization of thermal design parameters that affect the COMS temperature of the space-based EUV radiation detector of the LST, called the SCI121.6 detector. Figure 4C shows the structure of the SCI121.6 detector.

B. THERMOPHYSICAL MODEL OF THE LST

The thermophysical model of the spacecraft must be analyzed before IOSML can be applied to the thermal analysis of the LST. The node network methodology is a simplified finite difference method and the most commonly employed methodology for the thermo-physical modelling of spacecraft. In the thermal analysis of a spacecraft adopting node network methodology, the actual physical model of the spacecraft is divided into modules (i.e., nodes) of a certain size, and various thermal parameters in the modules are represented by centralized parameters represented by the nodes. The radiative, conductive, and convective heat transfer processes between nodes are respectively summarized as radiation network branches, conduction network branches, and convective network branches that connect the heat flow among nodes. According to its properties, the LST can be decomposed into several special finite units, each of which is considered an isothermal object. The thermophysical model is shown in Fig. 6.

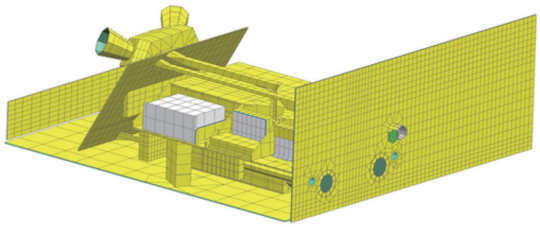

FIGURE 6. Thermophysical model of the LST.

Following the 3D model and thermal control scheme of the LST, the thermophysical model of the LST was built using NX TMG Thermal Analysis software, as shown in Fig. 6. The model has 53,970 cells, 55,874 nodes, and 236 thermal couplings and is referred to as a DTMM.

C. APPLICATION OF IOSML

1) SURROGATE MODEL BASED ON THE RBF-IMEA

In creating the training dataset for the surrogate model, we first sampled 5000 samples adopting LHS for 42 sets of parameters within their value ranges. The description and range of thermal design parameters are given in Table 4. We then input 80% of the samples into the IBPS as the training dataset for batch thermal analysis, 10% to verify the generality of the network, and the remaining 10% for testing. After all thermal analyses are complete, the IBPS stores all result data, especially the TD_CS and CMOS temperatures, in text format in the same Excel file in the specified path for training the surrogate model.

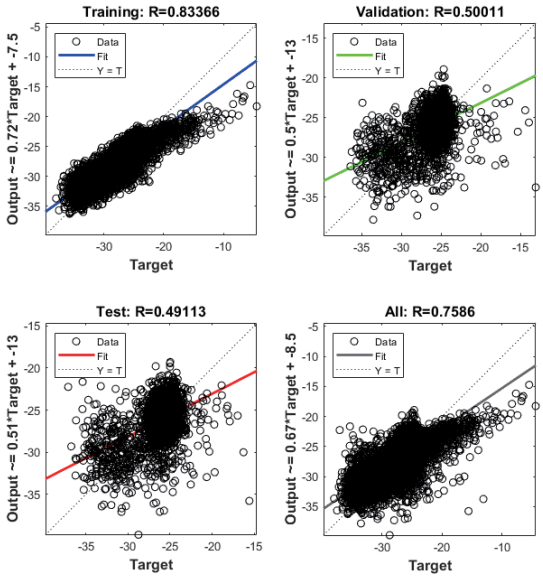

FIGURE 7. Regression of the established RBF NN without optimization in hot cases.

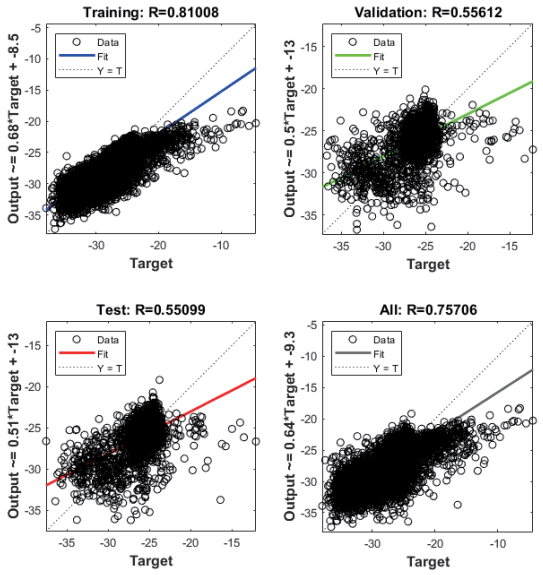

FIGURE 8. Regression of the established RBF NN without optimization in cold cases.

The RBF NN toolbox in MATLAB is used in this article, where the command 'newrbe' provides an automatic search for the optimal structure of the RBF NN. The specific node number and learning rate of the implicit layer are respectively taken as 71 and 0.1. After 474 iterations, the mean square error in training the RBF NN surrogate model is 5.9306, which is greater than the pre-defined training target of 1e-2 and does not meet the convergence requirement. As shown in the regression analysis of Figs. 7 and 8, the computational error between the RBF NN surrogate model and the traditional thermophysical model is still less than 85%, so the hyperparameters of the RBF NN must be optimized.

TABLE 4. Description and range of thermal design parameters.

	Parameter number	Description	Base value	Lower limit	Upper limit
Solar absorptivity	1	Inner surface of the cold cover	0.84	0.8	0.95
	2	Outer surface of the cold cover	0.25	0.15	0.4
	3	Radiation panel	0.18	0.12	0.25
	4	Inner surface of double layer insulating board	0.84	0.8	0.95
	5	Outer surface of double layer insulating board	0.25	0.15	0.4
	6	Inner surface of focal plane box	0.84	0.8	0.95
	7	F46	0.41	0.11	0.45
Infrared emissivity	8	Inner surface of the cold cover	0.84	0.8	0.95
	9	Outer surface of the cold cover	0.05	0.02	0.05
	10	Radiation panel	0.87	0.8	0.94
	11	Inner surface of double layer insulating board	0.84	0.8	0.95
	12	Outer surface of double layer insulating board	0.05	0.02	0.05
	13	Inner surface of focal plane box	0.84	0.8	0.95
	14	F46	0.68	0.6	0.8
Thermal resistance, $K \cdot W^{-1}$	15	Between thermal cable and thermal conductor	1.11	0.13	2.5
	16	Between thermal cable and cold cover	0.23	0.13	2.5
	17	Between thermal cable and heat pipe	1.23	0.13	2.5
	18	Between heat pipe and thermal cable	0.67	0.13	2.5
	19	Between thermal conductor and CMOS	4.22	1.48	4.44
	20	Between thermal conductor and focal plane box	1.18	0.71	3.53
	21	Between cold cover and insulation pads	3.79	2.28	25
	22	Between cold cover and PCB	201.81	21.4	273.14
	23	Between cold cover and double layer insulating board	68.42	3.98	81.68
	24	Between cold cover and focal plane box	11.74	1.86	38.01
	25	Between double layer insulating board and framework	68.42	3.98	81.68
	26	Between double layer insulating board and external insulation ring	5	0.63	10
	27	Between double layer insulating board and internal insulation ring	5	0.47	10
	28	Between external insulation ring and framework	15	2.5	25
	29	Between internal insulation ring and cold cover	5	2.1	10.47
	30	Between focal plane box and CMOS	6.93	4.16	40
	31	Between focal plane box and insulation pads	3.79	2.28	40
	32	Between focal plane box and press plate	3.89	2.34	40
	33	Between CMOS and press plate	12.15	7.29	66.67
	34	Between CMOS and PCB	4.47	2.68	13.42
Thickness, mm	35	Internal insulation ring	2.35	1	5
	36	External insulation ring	2.91	1	5
	37	Insulation pads	1.24	1	5
Heat transfer coefficient, $W \cdot m^{-1} \cdot K^{-1}$	38	Between multilayer and wrapped area	0.17	0.05	0.6
Thermal conductivity, $W \cdot m^{-2} \cdot K^{-1}$	39	Thermal conductor	154	100	250
	40	Thermal cable	300	150	300
	41	Cold cover	154	100	250
	42	Focal plane box	154	100	250

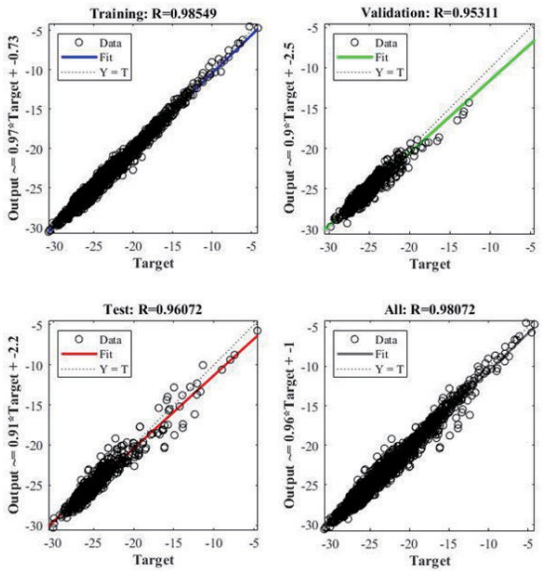

FIGURE 9. Regression of the established RBF-IMEA in the hot case.

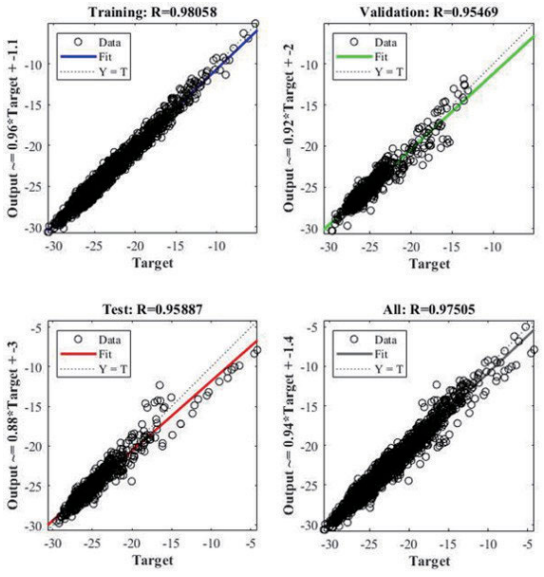

FIGURE 10. Regression of the established RBF-IMEA in the cold case.

As described in subsection 3.2, IMEA was employed to optimize the hyperparameters of the RBF NN surrogate model in this article. Finally, after 414 iterations of training and optimization, an RBF-IMEA neural network surrogate model with a structure of 42-71-1 was obtained, and its mean square error was reduced to 3.56e-3. Regression analysis of

TABLE 5. GSA of the SCI121.6 detector in the hot case.

	Main effect			Total effect		
No.	Median	Max	Min	Median	Max	Min
1	-0.0215	0.0063	-0.0287	0.0672	0.0736	0.0633
2	-0.0001	0.0166	-0.0048	0.0581	0.0654	0.0502
3	-0.0104	0.0123	-0.0228	0.0435	0.0482	0.0353
4	0.087	0.1052	0.0661	0.1457	0.1507	0.14
5	0.0582	0.0898	0.0536	0.1264	0.1324	0.1188
6	0.0022	0.0215	-0.0096	0.061	0.0678	0.0572
7	-0.0722	-0.0486	-0.0869	0.1715	0.1865	0.1527
8	0.0093	0.0125	-0.0109	0.0886	0.0946	0.0818
9	0.0268	0.0402	0.0178	0.0993	0.1051	0.093
10	0.0951	0.1195	0.0809	0.1635	0.1687	0.1573
11	-0.0365	-0.0208	-0.0536	0.0418	0.0476	0.0357
12	-0.0548	-0.0374	-0.0703	0.0134	0.0209	0.0078
13	-0.0241	0.0042	-0.0298	0.0382	0.0435	0.0301
14	0.0732	0.0904	0.0602	0.1366	0.142	0.1289
15	-0.0359	-0.0082	-0.0472	0.0215	0.0262	0.0131
16	-0.0149	0.0049	-0.0285	0.0327	0.0379	0.0249
17	0.001	0.0207	-0.0184	0.0528	0.057	0.0439
18	0.0561	0.08	0.0486	0.1189	0.1252	0.1146
19	-0.1833	-0.1587	-0.1988	0.0195	0.0377	0.0026
20	0.035	0.0625	0.0293	0.0938	0.0991	0.0865
21	0.0353	0.06	0.0261	0.094	0.0991	0.0874
22	0.0033	0.0275	-0.0095	0.0658	0.0711	0.0585
23	**0.4026**	**0.4289**	**0.3908**	**0.6313**	**0.6523**	**0.6178**
24	0.0921	0.1174	0.0863	0.1509	0.1562	0.1449
25	0.0916	0.1147	0.0849	0.1604	0.1655	0.1531
26	0.047	0.0667	0.0379	0.1157	0.1216	0.1091
27	0.0813	0.1015	0.0785	0.1577	0.1624	0.1503
28	0.0837	0.1037	0.075	0.1477	0.1531	0.1406
29	0.0663	0.0957	0.0656	0.121	0.1268	0.1143
30	-0.0259	0.0043	-0.0254	0.0453	0.0497	0.0372
31	0.0404	0.0614	0.0324	0.1078	0.1142	0.1027
32	0.011	0.0364	0.0053	0.0786	0.0839	0.0712
33	0.0608	0.091	0.0572	0.1232	0.1285	0.1161
34	**0.1187**	**0.1403**	**0.1101**	**0.3375**	**0.3574**	**0.3258**
35	-0.0779	-0.0599	-0.0901	0.0191	0.0252	0.0139
36	-0.0619	-0.0452	-0.0741	0.0069	0.011	-0.0012
37	-0.0069	0.011	-0.0195	0.0614	0.0655	0.0525
38	**0.7908**	**0.8162**	**0.7971**	**0.8654**	**0.8774**	**0.8618**
39	-0.0296	-0.0097	-0.043	0.0391	0.0442	0.0315
40	0.0996	0.1205	0.0998	0.3184	0.3374	0.3018
41	**0.1124**	**0.1371**	**0.1095**	**0.1811**	**0.1859**	**0.1736**
42	-0.0358	-0.006	-0.0396	0.0406	0.0449	0.0336

TABLE 6. GSA of the SCI121.6 detector in the cold case.

	Main effect			Total effect		
No.	Median	Max	Min	Median	Max	Min
1	-0.0173	0.0033	-0.0261	0.0537	0.0696	0.0479
2	-0.0007	0.0203	-0.0037	0.0436	0.0579	0.0396
3	-0.0113	0.0106	-0.0243	0.0397	0.0406	0.0291
4	0.0716	0.1104	0.0451	0.1206	0.1309	0.0907
5	0.0509	0.0817	0.0475	0.1104	0.1231	0.1001
6	0.0019	0.0996	-0.099	0.0582	0.0589	0.0579
7	-0.0732	-0.0463	-0.0896	0.1537	0.1965	0.1357
8	0.0075	0.0108	-0.0112	0.0773	0.0842	0.0613
9	0.0297	0.0537	0.0218	0.0997	0.1106	0.0965
10	0.0763	0.0964	0.0632	0.1308	0.1541	0.1024
11	-0.0401	-0.0278	-0.0539	0.0394	0.0456	0.0307
12	-0.0531	-0.0351	-0.0693	0.0128	0.0278	0.0042
13	-0.0232	0.0044	-0.0287	0.0307	0.0421	0.0284
14	0.0851	0.1004	0.0799	0.1457	0.1596	0.1352
15	-0.0312	-0.0078	-0.0501	0.0198	0.0259	0.0176
16	-0.0155	0.0031	-0.0315	0.0276	0.0534	0.0138
17	0.0003	0.0197	-0.0106	0.0351	0.056	0.0201
18	0.0653	0.0911	0.0517	0.1357	0.1769	0.1005
19	-0.2019	-0.1918	-0.2024	0.0113	0.0269	0.001
20	0.0276	0.0549	0.0199	0.0794	0.1009	0.0439
21	0.0367	0.0712	0.0293	0.0974	0.1012	0.0938
22	0.0021	0.0214	-0.0105	0.0567	0.0675	0.0491
23	**0.5316**	**0.6107**	**0.4531**	**0.6927**	**0.7291**	**0.5911**
24	0.0815	0.1012	0.0764	0.1351	0.1713	0.1131
25	0.091	0.1094	0.0768	0.1583	0.1754	0.1315
26	0.0431	0.0766	0.0363	0.1003	0.1415	0.0916
27	0.0828	0.1167	0.0702	0.1666	0.1721	0.1545
28	0.081	0.1322	0.0704	0.1399	0.1601	0.1333
29	0.0593	0.09	0.0569	0.1038	0.1381	0.0948
30	-0.0244	0.0049	-0.0197	0.0411	0.0512	0.025
31	0.0395	0.0576	0.0246	0.1001	0.1238	0.0933
32	0.0127	0.0389	0.0042	0.0684	0.0935	0.0546
33	0.0661	0.1039	0.0751	0.14	0.1538	0.1329
34	**0.1301**	**0.1512**	**0.1237**	**0.4354**	**0.6574**	**0.3782**
35	-0.0702	-0.0601	-0.0832	0.0165	0.0199	0.0151
36	-0.0598	-0.0352	-0.0682	0.0073	0.0201	-0.0017
37	-0.0072	0.0096	-0.0206	0.0539	0.0596	0.0491
38	**0.8694**	**0.9348**	**0.6895**	**0.9041**	**0.9768**	**0.8359**
39	-0.0216	-0.0069	-0.025	0.0405	0.0476	0.0355
40	0.096	0.1035	0.0812	0.3029	0.3451	0.2918
41	**0.1416**	**0.1764**	**0.1219**	**0.2031**	**0.2511**	**0.1817**
42	-0.0179	-0.011	-0.0281	0.049	0.0502	0.0379

the proposed RBF-IMEA surrogate model in both hot and cold cases shows that the model accurately reflects the functional relationship between the TD_CS and 42 parameters (see Figs. 9 and 10). Additionally, the RBF-IMEA surrogate model has a computational speed 100+ times faster than that of the traditional thermophysical model and a high computational accuracy of 95%+.

2) GSA OF THERMAL DESIGN PARAMETERS OF THE LST

Once the RBF-IMEA neural network surrogate model is obtained, the second stage begins (see Section 3.4). Table 5 shows that the difference between the maximum and minimum values of the density-based GSA for the effects of 42 thermal design parameters of the SCI121.6 detector on the CMOS temperature in the hot case does not exceed 0.05 when the computational cost reaches 5000, satisfying the accuracy requirements of the GSA for the initial thermal design parameters of the LST. Additionally, the density-based GSA for the effect of 42 thermal design parameters of the SCI121.6 detector on the CMOS temperature in the cold case, shown in Table 6, satisfies the accuracy requirements of the GSA for the initial thermal design parameters of the LST.

The main effect refers to each input factor's main contribution to the output variance. The total effect explains the total contribution of all higher-order effects to the output variance due to the main effect and interactions between different inputs. It is clear from Table 5 that in the hot case, the main effect and the total effect of Parameters 23, 34, 38, and 41 are higher than those of other parameters. Their GSA values exceed 0.1, while almost all other parameters have GSA values below 0.1. Parameters 23, 34, 38, and 41 are the four parameters that largely affect the CMOS temperature, while other parameters have a smaller effect. Sixteen of the forty-two parameters have a main effect less than zero, which indicates that they have a small effect on the CMOS temperature and are insensitive to the CMOS temperature

TABLE 7. Number of optimization iterations and results in the hot case.

	Iterations of optimization and results									
No.	1	2	3	.....	8	9	10	.....	14	15	16
1	0.8626	0.8502	0.9245	.....	0.8952	0.8973	0.8574	.....	0.8	0.8	0.8
2	0.908	0.8573	0.8774	.....	0.9495	0.8033	0.8033	.....	0.8	0.8	0.8
3	0.15	0.2317	0.3282	.....	0.1608	0.1574	0.3491	.....	0.15	0.15	0.15
4	0.0291	0.0371	0.0326	.....	0.0438	0.0444	0.0499	.....	0.02	0.02	0.02
5	0.1391	0.1694	0.2299	.....	0.2496	0.1619	0.1316	.....	0.25	0.25	0.25
6	0.8129	0.8325	0.8584	.....	0.8514	0.9159	0.8745	.....	0.8	0.94	0.94
7	0.8279	0.9	0.8717	.....	0.9151	0.8693	0.9459	.....	0.8	0.8	0.8
8	0.8518	0.899	0.8802	.....	0.8419	0.8672	0.9334	.....	0.8	0.8	0.8
9	0.2492	0.2403	0.3384	.....	0.3495	0.2942	0.2815	.....	0.4	0.4	0.4
10	0.0362	0.0241	0.0251	.....	0.0457	0.0345	0.0411	.....	0.02	0.02	0.02
11	0.8629	0.8138	0.9423	.....	0.9242	0.8876	0.9243	.....	0.95	0.95	0.95
12	0.9028	0.8002	0.8208	.....	0.9326	0.8852	0.8629	.....	0.8	0.8	0.8
13	0.1795	0.3702	0.1516	.....	0.3746	0.2377	0.142	.....	0.11	0.11	0.11
14	0.7756	0.6312	0.7225	.....	0.6437	0.6317	0.794	.....	0.6	0.6	0.6
15	0.1949	2.1813	0.5345	.....	2.4215	2.4202	2.377	.....	2.5	2.5	2.5
16	1.719	1.0801	0.9701	.....	1.2632	1.9416	1.0667	.....	0.13	0.13	0.13
17	1.119	1.0502	0.673	.....	1.3478	1.4888	1.2523	.....	2.5	2.5	2.5
18	1.4541	0.2799	0.5694	.....	0.9993	0.13	0.8716	.....	0.13	0.13	0.13
19	1.8955	2.0736	2.9621	.....	3.1129	2.3862	4.0139	.....	4.44	4.44	4.44
20	1.2686	2.3324	1.8635	.....	1.8381	3.2504	2.2039	.....	0.71	0.71	0.71
21	20.4729	16.7171	16.4428	.....	7.1468	8.3111	8.9266	.....	11.0352	9.2011	9.2691
22	265.1502	184.6465	230.1576	.....	211.8595	226.8778	211.3097	.....	92.0414	91.0146	90.5138
23	**28.3331**	**47.2295**	**49.3651**	**.....**	**64.429**	**68.8995**	**53.0187**	**.....**	**68.2089**	**69.0543**	**68.3816**
24	26.8875	26.5211	25.7576	.....	35.9847	35.8912	30.5488	.....	30.5198	32.5508	30.8786
25	72.0754	73.6877	24.2902	.....	15.121	29.1239	35.9331	.....	36.7412	34.8337	35.7461
26	9.0125	2.3667	3.5407	.....	3.2543	8.1822	2.8874	.....	8.4037	7.496	8.4556
27	1.2805	7.1904	4.5416	.....	3.5697	6.0761	8.3709	.....	8.0416	7.8665	5.8252
28	3.3787	24.3101	22.1698	.....	22.181	20.7353	24.8182	.....	18.2339	19.1437	19.7137
29	3.5215	10.2173	7.7311	.....	8.4411	9.4365	4.0222	.....	4.4936	3.2499	3.2044
30	35.6326	7.9241	32.502	.....	31.7831	24.8823	33.1054	.....	30.1173	29.7792	29.2504
31	5.9896	38.0167	31.7635	.....	39.1866	31.2306	33.8826	.....	32.4118	33.7347	34.4299
32	18.1989	11.0237	14.6038	.....	29.1464	36.3241	21.1655	.....	11.6982	10.8218	10.5139
33	64.1695	60.2404	40.0876	.....	43.0886	50.3036	54.2294	.....	36.4348	32.9744	34.3483
34	**8.4062**	**10.5679**	**9.9553**	**.....**	**6.4941**	**6.8894**	**3.2998**	**.....**	**6.8669**	**5.9038**	**8.064**
35	3.7675	2.7901	3.57	.....	1.8431	3.1534	1.3201	.....	1	1	1
36	2.2621	4.7509	4.2509	.....	2.5749	3.2454	2.7758	.....	3.6909	2.2888	2.3657
37	3.746	1.3583	3.675	.....	2.6013	3.1952	4.2999	.....	5	5	5
38	**0.1752**	**0.0547**	**0.1653**	**.....**	**0.1768**	**0.2**	**0.1636**	**.....**	**0.2**	**0.2**	**0.2**
39	135.1264	207.3651	169.3541	.....	106.7538	147.3329	154.5162	.....	154.5162	154.5162	154.5162
40	**178.9613**	**199.3846**	**186.2684**	**.....**	**278.3591**	**225.3794**	**232.3719**	**.....**	**235.4682**	**235.4682**	**235.4682**
41	145.9218	155.6792	181.3574	.....	159.3412	166.9534	176.3984	.....	182.3351	182.3351	182.3351
42	165.3329	135.2645	200.3768	.....	189.1128	184.6549	180.5294	.....	201.1684	201.1684	201.1684
CMOS	**-24.525**	**-24.864**	**-25.222**	**.....**	**-25.726**	**-26.186**	**-26.61**	**.....**	**-26.716**	**-26.176**	**-26.034**
TD_CS	**0.671**	**1.547**	**2.041**	**.....**	**4.275**	**5.004**	**5.394**	**.....**	**7.35**	**7.658**	**7.756**

and can thus be ignored when optimizing the thermal design parameters of the LST.

Comparing the effects of each thermal design parameter on the CMOS temperature in the hot and cold cases(see Table 6), the trends are similar, and only a few individual parameters have conflicting results. Additionally, the degree of the effect on the CMOS temperature is relatively similar. As an example, the main effect and total effect of Parameters 23 and 38 on the CMOS temperature are respectively 0.4026, 0.6313 and 0.7908, 0.8654 in the hot case and 0.5316, 0.6927 and 0.8694, 0.9041 in the cold case. The main reason for the similar trends with little difference in GSA is that there is little difference in the beta angle between hot and cold cases. The beta angle is the angle between the sunlight and orbital plane, which greatly affects the solar radiation received by the space telescope and thus the overall temperature distribution of the space telescope. The above analysis clearly shows that Parameters 23, 34, 38, and 41 are the four parameters that strongly affect the CMOS temperature and require attention in the optimization of LST thermal design parameters.

3) BAYESIAN OPTIMIZATION OF THERMAL DESIGN PARAMETERS OF THE LST

Once the four important parameters that appreciably affect the CMOS temperature are acquired through the GSA of the LST thermal design parameters, the last but critical step of the second phase begins—the optimization of the LST thermal design parameters adopting the Bayesian optimization algorithm.

Table 7 presents the numbers of optimized iterations and results of IOSML in the hot case with no supervision. As the number of optimized iterations increases, the CMOS

TABLE 8. Number of optimization iterations and results in the cold case.

	Iterations of optimization and results										
No.	1	2	3	.....	8	9	10	.....	14	15	16
1	0.9178	0.9461	0.9102	.....	0.8	0.8441	0.8	.....	0.8881	0.95	0.95
2	0.8785	0.9288	0.9117	.....	0.95	0.8823	0.8	.....	0.8762	0.8	0.8
3	0.2425	0.3116	0.2978	.....	0.3799	0.1761	0.15	.....	0.3512	0.15	0.15
4	0.0248	0.0449	0.0476	.....	0.0323	0.0493	0.0323	.....	0.0363	0.05	0.02
5	0.1267	0.2443	0.2104	.....	0.25	0.2201	0.25	.....	0.2148	0.25	0.25
6	0.8258	0.8443	0.8881	.....	0.94	0.9129	0.94	.....	0.9395	0.94	0.94
7	0.8565	0.8631	0.8213	.....	0.9392	0.8978	0.9159	.....	0.8414	0.8	0.8
8	0.8926	0.8819	0.9101	.....	0.9499	0.95	0.95	.....	0.901	0.8	0.8
9	0.3239	0.2491	0.385	.....	0.4	0.2693	0.4	.....	0.3161	0.15	0.4
10	0.0429	0.0359	0.0243	.....	0.05	0.0262	0.05	.....	0.0396	0.05	0.02
11	0.8193	0.8233	0.9089	.....	0.95	0.9464	0.95	.....	0.8353	0.8	0.95
12	0.876	0.899	0.8951	.....	0.8088	0.864	0.8	.....	0.9223	0.95	0.8
13	0.4273	0.4151	0.1243	.....	0.45	0.45	0.45	.....	0.2771	0.11	0.11
14	0.6871	0.6813	0.7737	.....	0.8	0.7465	0.6923	.....	0.633	0.6	0.6
15	1.1796	0.9124	2.3927	.....	1.6352	2.5	2.5	.....	2.5	2.5	2.5
16	1.5147	1.3625	1.1615	.....	0.13	0.5616	0.13	.....	0.7154	0.13	0.13
17	1.117	1.6688	1.9771	.....	2.5	2.5	2.5	.....	2.4544	2.5	2.5
18	0.4899	1.0905	1.0588	.....	2.5	1.3296	2.5	.....	0.2857	0.13	0.13
19	3.2839	4.2702	4.2085	.....	2.63	3.3454	4.44	.....	3.7856	4.44	4.44
20	2.7598	1.2376	1.7687	.....	2.937	0.71	0.71	.....	3.53	1.3387	0.71
21	3.9348	9.3653	23.7882	.....	2.2832	6.2748	2.5015	.....	11.4582	11.0358	8.1573
22	147.9892	107.3102	65.1003	.....	268.0917	148.7716	263.8501	.....	118.2579	116.9595	92.3079
23	**58.3931**	**66.05**	**73.5275**	**.....**	**81.68**	**32.7455**	**81.68**	**.....**	**67.1993**	**72.5441**	**67.7195**
24	22.6348	35.9152	3.1652	.....	14.4616	22.2468	14.1332	.....	27.9777	30.0447	30.7839
25	64.2194	38.9379	51.269	.....	64.2573	42.0935	65.9276	.....	50.141	46.2426	33.8259
26	6.4105	1.8518	6.5203	.....	0.8858	7.1503	10	.....	8.1737	9.4449	8.9207
27	8.8064	9.3031	1.3791	.....	0.47	10	0.47	.....	7.8009	8.3004	6.4554
28	4.6792	21.2579	17.7441	.....	24.9894	3.5269	25	.....	13.4578	13.8685	18.2184
29	9.8598	5.5867	7.3242	.....	10.47	2.7113	10.47	.....	6.2039	5.1919	3.792
30	35.9713	7.3908	25.7976	.....	11.4161	40	19.6873	.....	19.4563	19.4455	30.8474
31	20.2892	9.3299	38.4598	.....	14.7857	14.6653	19.5958	.....	28.6011	28.8182	32.1223
32	33.7097	30.7129	14.9329	.....	39.5204	39.5881	40	.....	12.8371	12.285	11.8132
33	12.7463	32.2578	53.9487	.....	53.6881	16.2848	51.038	.....	54.3147	54.4072	34.955
34	**12.2942**	**6.4745**	**7.8067**	**.....**	**7.7499**	**4.0994**	**13.42**	**.....**	**9.3528**	**12.3734**	**7.5484**
35	4.8795	3.2643	4.1713	.....	1.4288	1.2968	4.395	.....	1	1	1
36	2.5046	4.3425	2.1565	.....	3.0674	1.2508	5	.....	3.6225	2.7161	3.7234
37	3.7667	3.101	4.9642	.....	2.6596	3.7401	5	.....	3.5893	1	5
38	**0.0679**	**0.1301**	**0.1153**	**.....**	**0.2**	**0.2**	**0.2**	**.....**	**0.2**	**0.2**	**0.2**
39	166.1957	170.2155	161.3591	.....	189.3251	188.5138	215.2846	.....	205.3168	192.5543	205.3168
40	**191.5753**	**199.1683**	**184.3915**	**.....**	**205.3846**	**210.3351**	**246.2251**	**.....**	**275.9436**	**268.3951**	**275.9436**
41	132.4967	155.3376	149.1765	.....	199.0305	235.6814	201.3855	.....	210.2267	207.3154	210.2267
42	129.4916	176.4493	146.5252	.....	189.3245	197.2258	190.6659	.....	199.8802	175.446	199.8802
CMOS	**-24.776**	**-25.188**	**-25.084**	**.....**	**-25.402**	**-25.688**	**-26.366**	**.....**	**-26.589**	**-26.188**	**-26.035**
TD_CS	**0.189**	**1.464**	**1.801**	**.....**	**4.145**	**5.033**	**5.348**	**.....**	**7.29**	**7.575**	**7.706**

temperature remains within the range of 30 to 25°C, and the TD_CS value has an increasing trend. After nine iterations, the TD_CS is greater than 5°C, meeting the requirements of LST thermal control.

Similarly, as shown in Table 8, the TD_CS can exceed 5°C after nine optimization iterations, and the CMOS temperature meets the thermal control specifications.

D. RESULITS

To compare the optimization performance of GA, PSO, and POW with that of IOSML proposed in this article, four major factors are selected as the main optimization parameters from the density-based GSA (Parameter 23: thermal resistance between the cold cover and double-layer insulating board; Parameter 34: thermal resistance between the CMOS and printed circuit board (PCB); Parameter 38: coefficient of heat transfer between the multiple layers and wrapped area; and Parameter 41: thermal conductivity of the cold cover), and the remaining parameters are used as supplementary optimization parameters. One-hundred unsupervised iterations of optimization are then performed using each algorithm separately through the IBPS. Detailed information of the parameters for the four algorithms are given in Table 9.

Figure 11 shows that, after nine optimized iterations of IOSML in the hot case, the TD_CS of the SCI121.6 detector onboard the LST meets the requirement of thermal control (i.e., the TD_CS temperature always exceeds 5°C when the CMOS temperature is precisely controlled from 30 to 25°C), which is better than the performance of the GA, PSO, and POW. Indeed, after nine iterations, the GA, PSO and POW only control the temperature of the CMOS within the temperature range required for thermal control, while the TD_CS temperature is still far from standard. Only after at least 60 optimization iterations do the latter three algorithms meet

TABLE 9. Detailed information of parameters for the four algorithms.

Category	Information of parameters
IOSML	Hyper-parameters for optimization = 2.5
GA	The number of evolutions is 100 The population size is 20 Crossover probability is taken as 0.4 Mutation probability equal to 0.2
PSO	The number of particles in the population is 20 The dimension of a single particle is 2 The number of iterative evolutions of the algorithm is taken as 100
POW	The initial parameter k=1 The accuracy standard is set to 0.1

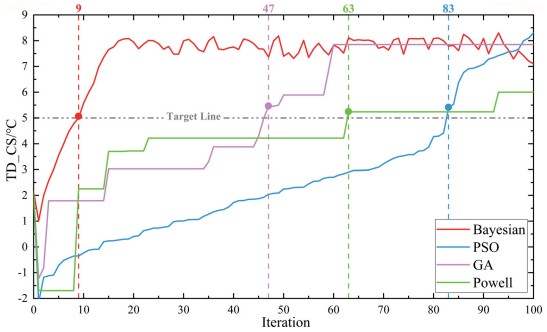

FIGURE 11. Comparison of optimization performance in the hot case.

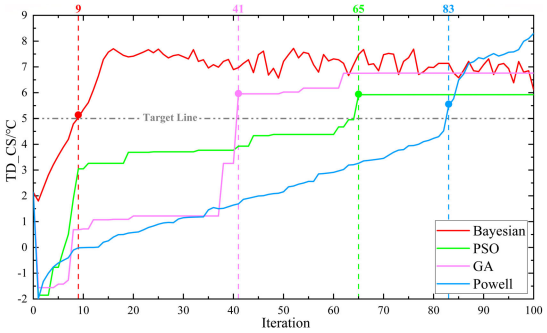

FIGURE 12. Comparison of optimization performance in the cold case.

the requirements of thermal control. IOSML is thus at least twice as efficient as the other methods.

Figure 12 shows that, similar to the optimization procedure in the cold case, after nine iterations based on IOSML, the TD_CS of the SCI121.6 detector onboard the LST also meets the requirements of thermal control. However, the convergences of the GA, PSO, and POW are slow. It is clear that IOSML not only greatly improves the efficiency of optimization of thermal design parameters but also ensures that the CMOS temperature is unaffected by the optimization process, allowing unsupervised multi-objective optimization.

The efficiency of the optimization of thermal design parameters based on statistical machine learning proposed in this article is limited by the computational resources used (Intel Core i9-9900X CPU, 64GB RAM, GeForce RTX 2080 Ti), which directly affects the time required for model calculation. With the further improvement of computational resources, the calculation time of the model evaluation and GSA will be shortened, further promoting the application of IOSML in the thermal design parameter optimization task of a space telescope.

V. CONCLUSION

An intelligent optimization strategy based on statistical machine learning for spacecraft thermal design was proposed. The strategy uses an RBF-IMEA neural network surrogate model to reduce the computational cost of model evaluation, while accuracy is maintained by constructing a training dataset for the RBF-IMEA neural network surrogate model with a DTMM. Additionally, an intelligent batch thermal analysis system was designed specifically for the present study, allowing the unsupervised transfer of textual command data and analysis result data between the various software programs through real-time data interaction between MATLAB and NX TMG Thermal Analysis software.

In the specific application process, the RBF-IMEA neural network surrogate model was first applied to approximate the thermophysical model of the space telescope; the important factors affecting the CMOS temperature of the SCI121.6 detector onboard the LST were then identified adopting density-based GSA via the IBPS. Optimization adopting the Bayesian optimization algorithm was finally carried out.

Both theoretical and experimental results show that the optimization of thermal design parameters based on IOSML is better than optimization adopting traditional methods such as the use of a GA, PSO, or POW, achieving better model evaluation accuracy and higher calculation efficiency. It is crucial that the entire process be automated to help avoid human errors and thus improve the efficiency of the thermal design optimization for space telescopes. Moreover, it is obvious that the intelligent optimization strategy proposed in this article is applicable not only to the optimization of thermal design parameters of space telescopes but also to post-processing and design optimization in other fields.

Additionally, the convergence of IOSML is not particularly stable and there is random fluctuation because the process involved in engineering applications is complex. To further improve the thermal design of space telescopes, it is essential to further improve the convergence effect and simplify the implementation process of IOSML.

ACKNOWLEDGMENT

The authors thank Prof. Christos N. Markides from the Clean Energy Processes (CEP) Laboratory, Department of Chemical Engineering, Imperial College London, U.K., for providing valuable guidance and suggestions for this research.

REFERENCES

[1] D. G. Gilmore and M. Donabedian, *Spacecraft Thermal Control Handbook: Cryogenics*. Reston, VA, USA: American Institute of Aeronautics and Astronautics, 2003, doi: 10.2514/4.989148.

[2] R. Nie, B. He, S. Yan, and X. Ma, "Optimization design method for the cable network of mesh reflector antennas considering space thermal effects," *Aerosp. Sci. Technol.*, vol. 94, Nov. 2019, Art. no. 105380, doi: 10.1016/j.ast.2019.105380.

[3] R. L. Galski, F. L. De Sousa, F. M. Ramos, and I. Muraoka, "Spacecraft thermal design with the generalized extremal optimization algorithm," *Inverse Problems Sci. Eng.*, vol. 15, no. 1, pp. 61–75, Jan. 2007, doi: 10.1080/17415970600573924.
[4] I. Muraoka, R. L. Galski, F. L. de Sousa, and F. M. Ramos, "Stochastic spacecraft thermal design optimization with low computational cost," *J. Spacecraft Rockets*, vol. 43, no. 6, pp. 1248–1257, Nov. 2006, doi: 10.2514/1.20066.
[5] D. Whitley, "A genetic algorithm tutorial," *Statist. Comput.*, vol. 4, no. 2, pp. 65–85, Jun. 1994, doi: 10.1007/BF00175354.
[6] S. N. Sivanandam and S. N. Deepa, "Genetic algorithm optimization problems," in *Introduction to Genetic Algorithms*. Berlin, Germany: Springer, 2008, pp. 165–209, doi: 10.1007/978-3-540-73190-0_7.
[7] H.-Y. Tang, H.-Y. Ye, X.-P. Chen, C. Qian, X.-J. Fan, and G.-Q. Zhang, "Numerical thermal analysis and optimization of multi-chip LED module using response surface methodology and genetic algorithm," *IEEE Access*, vol. 5, pp. 16459–16468, 2017, doi: 10.1109/ACCESS.2017.2737638.
[8] X. Kuang, K. Li, Y. Xie, C. Wu, P. Wang, X. Wang, and C. Fu, "Research on control strategy for a battery thermal management system for electric vehicles based on secondary loop cooling," *IEEE Access*, vol. 8, pp. 73475–73493, 2020, doi: 10.1109/ACCESS.2020.2986814.
[9] S. Rana, S. Jasola, and R. Kumar, "A review on particle swarm optimization algorithms and their applications to data clustering," *Artif. Intell. Rev.*, vol. 35, no. 3, pp. 211–222, Mar. 2011, doi: 10.1007/s10462-010-9191-9.
[10] L. Zhihuan, L. Yinhong, and D. Xianzhong, "Non-dominated sorting genetic algorithm-II for robust multi-objective optimal reactive power dispatch," *IET Gener., Transmiss. Distrib.*, vol. 4, no. 9, pp. 1000–1008, 2010, doi: 10.1049/iet-gtd.2010.0105.
[11] R. H. Myers, D. C. Montgomery, and C. M. Anderson-Cook, *Response Surface Methodology: Process and Product Optimization Using Designed Experiments*. Hoboken, NJ, USA: Wiley, 2016.
[12] S. Rahmani, M. Ebrahimi, and A. Honaramooz, "A surrogate-based optimization using polynomial response surface in collaboration with population-based evolutionary algorithm," in *Proc. World Congr. Struct. Multidisciplinary Optim.*, 2017, pp. 269–280, doi: 10.1007/978-3-319-67988-4_19.
[13] A. Saltelli, M. Ratto, T. Andres, F. Campolongo, J. Cariboni, D. Gatelli, M. Saisana, S. Tarantola, *Global Sensitivity Analysis: The Primer*. Hoboken, NJ, USA: Wiley, 2008.
[14] F. Yuan, B. Tang, C. Ding, S. Qin, L. Huang, and Z. Yuan, "Optimization design of a high-coupling split reactor in a parallel-type circuit breaker," *IEEE Access*, vol. 7, pp. 33473–33480, 2019, doi: 10.1109/ACCESS.2019.2900697.
[15] T. J. R. Hughes, *The Finite Element Method: Linear Static and Dynamic Finite Element Analysis*. Chelmsford, MA, USA: Courier Corporation, 2012.
[16] B. M. Kim and S. J. Yoo, "Approximation-based adaptive control of constrained uncertain thermal management systems with nonlinear coolant circuit dynamics of PEMFCs," *IEEE Access*, vol. 8, pp. 83483–83494, 2020, doi: 10.1109/ACCESS.2020.2992047.
[17] M. Soltani, R. Kulkarni, T. Scheinost, T. Groezinger, and A. Zimmermann, "A novel approach for reliability investigation of LEDs on molded interconnect devices based on FE-analysis coupled to injection molding simulation," *IEEE Access*, vol. 7, pp. 56163–56173, 2019, doi: 10.1109/ACCESS.2019.2913786.
[18] M. Awad, R. Khanna, "Support vector regression," in *Efficient Learning Machines*. Berkeley, CA, USA: Apress, 2015, pp. 67–80, doi: 10.1007/978-1-4302-5990-9_4.
[19] J. H. Kim and B. Kim, "Study on the reduction method of the satellite thermal mathematical model," *Adv. Eng. Softw.*, vol. 108, pp. 37–47, Jun. 2017, doi: 10.1016/j.advengsoft.2017.02.007.
[20] S. Arabaci and E. Dirgin, "Thermal mathematical model correlation of an Earth observation satellite," in *Proc. 7th Int. Conf. Recent Adv. Space Technol. (RAST)*, Jun. 2015, pp. 439–442, doi: 10.1109/RAST.2015.7208385.
[21] J. Wu, X. Han, and H. Wang, "Electro-thermal modeling and design of high-current pulse power supply for electrically assisted manufacturing," *IEEE Access*, vol. 7, pp. 160377–160384, 2019, doi: 10.1109/ACCESS.2019.2949586.
[22] I. Torralbo, I. Perez-Grande, A. Sanz-Andres, and J. Piqueras, "Correlation of spacecraft thermal mathematical models to reference data," *Acta Astronautica*, vol. 144, pp. 305–319, Mar. 2018, doi: 10.1016/j.actaastro.2017.12.033.
[23] H. Azarkish and M. Rashki, "Reliability and reliability-based sensitivity analysis of shell and tube heat exchangers using Monte Carlo simulation," *Appl. Thermal Eng.*, vol. 159, Aug. 2019, Art. no. 113842, doi: 10.1016/j.applthermaleng.2019.113842.
[24] K. Stout. *Bayesian-Based Simulation Model Validation for Spacecraft Thermal Systems*. Accessed: Nov. 25, 2019. [Online]. Available: https://dspace.mit.edu/handle/1721.1/97358
[25] J. Snoek, H. Larochelle, and R. P. Adams, "Practical Bayesian optimization of machine learning algorithms," in *Proc. Adv. Neural Inf. Process. Syst.*, 2012, pp. 2951–2959.
[26] I. Dewancker, M. McCourt, S. Clark. *Bayesian Optimization Primer*. Accessed: Nov. 25, 2019. [Online]. Available: https://sigopt.com/research
[27] P. I. Frazier, "A tutorial on Bayesian optimization," 2018, *arXiv:1807.02811*. [Online]. Available: http://arxiv.org/abs/1807.02811
[28] H. Yang, J. Wen, S. Wang, and Y. Li, "Thermal design and optimization of plate-fin heat exchangers based global sensitivity analysis and NSGA-II," *Appl. Thermal Eng.*, vol. 136, pp. 444–453, May 2018, doi: 10.1016/j.applthermaleng.2018.03.035.
[29] W. Tian, C. Jiang, B. Ni, Z. Wu, Q. Wang, and L. Yang, "Global sensitivity analysis and multi-objective optimization design of temperature field of sinter cooler based on energy value," *Appl. Thermal Eng.*, vol. 143, pp. 759–766, Oct. 2018, doi: 10.1016/j.applthermaleng.2018.08.006.
[30] K. J. Knutson and C. Briggs, "Innovative computing techniques for NX Analysis and post processing to fill emerging needs," Jet Propuls. Lab., California Inst. Technol., Pasadena, CA, USA, Tech. Rep., 2005.
[31] M. Deiml, M. Suderland, P. Reiss, and M. Czupalla, "Development and evaluation of thermal model reduction algorithms for spacecraft," *Acta Astronautica*, vol. 110, pp. 168–179, May 2015, doi: 10.1016/j.actaastro.2015.01.018.
[32] D. A. White, W. J. Arrighi, J. Kudo, and S. E. Watts, "Multiscale topology optimization using neural network surrogate models," *Comput. Methods Appl. Mech. Eng.*, vol. 346, pp. 1118–1135, Apr. 2019, doi: 10.1016/j.cma.2018.09.007.
[33] D. Zhao, D. Liu, and M. Zhu, "A surrogate model for thermal characteristics of stratospheric airship," *Adv. Space Res.*, vol. 61, no. 12, pp. 2989–3001, Jun. 2018, doi: 10.1016/j.asr.2018.03.036.
[34] M. J. Asher, B. F. W. Croke, A. J. Jakeman, and L. J. M. Peeters, "A review of surrogate models and their application to groundwater modeling," *Water Resour. Res.*, vol. 51, no. 8, pp. 5957–5973, Aug. 2015, doi: 10.1002/2015WR016967.
[35] B. Shahriari, K. Swersky, Z. Wang, R. P. Adams, and N. de Freitas, "Taking the human out of the loop: A review of Bayesian optimization," *Proc. IEEE*, vol. 104, no. 1, pp. 148–175, Jan. 2016, doi: 10.1109/JPROC.2015.2494218.
[36] W. Lyu, P. Xue, F. Yang, C. Yan, Z. Hong, X. Zeng, and D. Zhou, "An efficient Bayesian optimization approach for automated optimization of analog circuits," *IEEE Trans. Circuits Syst. I, Reg. Papers*, vol. 65, no. 6, pp. 1954–1967, Jun. 2018, doi: 10.1109/TCSI.2017.2768826.
[37] S. J. Park, H. Yu, and M. Swaminathan, "Preliminary application of machine-learning techniques for thermal-electrical parameter optimization in 3-D IC," in *Proc. IEEE Int. Symp. Electromagn. Compat. (EMC)*, Jul. 2016, pp. 402–405, doi: 10.1109/ISEMC.2016.7571681.
[38] H. M. Torun, M. Swaminathan, A. Kavungal Davis, and M. L. F. Bellaredj, "A global Bayesian optimization algorithm and its application to integrated system design," *IEEE Trans. Very Large Scale Integr. (VLSI) Syst.*, vol. 26, no. 4, pp. 792–802, Apr. 2018, doi: 10.1109/TVLSI.2017.2784783.
[39] A. Rahman and A. D. Smith, "Predicting heating demand and sizing a stratified thermal storage tank using deep learning algorithms," *Appl. Energy*, vol. 228, pp. 108–121, Oct. 2018, doi: 10.1016/j.apenergy.2018.06.064.
[40] J. González, Z. Dai, P. Hennig, and N. Lawrence, "Batch Bayesian optimization via local penalization," in *Proc. 19th Int. Conf. Artif. Intell. Statist. (AISTATS)*, vol. 41. Cadiz, Spain: JMLR:W&CP, 2016, pp. 648–657.
[41] C. E. Rasmussen, "Gaussian processes in machine learning," in *Summer School on Machine Learning*. Berlin, Germany: Springer, 2003, pp. 63–71.
[42] J. C. Helton and F. J. Davis, "Latin hypercube sampling and the propagation of uncertainty in analyses of complex systems," *Rel. Eng. Syst. Saf.*, vol. 81, no. 1, pp. 23–69, 2003, doi: 10.1016/S0951-8320(03)00058-9.
[43] D. E. Huntington and C. S. Lyrintzis, "Improvements to and limitations of Latin hypercube sampling," *Probabilistic Eng. Mech.*, vol. 13, no. 4, pp. 245–253, 1998, doi: 10.1016/S0266-8920(97)00013-1.
[44] A. Humphrey, T. Harman, M. Berzins, and P. Smith, "A scalable algorithm for radiative heat transfer using reverse Monte Carlo ray tracing," in *Proc. Int. Conf. High Perform. Comput.*, 2015, pp. 212–230, doi: 10.1007/978-3-319-20119-1_16.

[45] D.-C. Yang, I.-S. Jang, M.-H. Jang, C.-N. Park, C.-J. Park, and J. Choi, "Optimization of additive compositions for anode in ni-MH secondary battery using the response surface method," *Met. Mater. Int.*, vol. 15, no. 3, pp. 421–425, Jun. 2009.

[46] M. D. Buhmann, "Radial basis functions," *Acta Numerica*, vol. 9, pp. 1–38, Jan. 2000.

[47] A. J. Smola and B. Schölkopf, "A tutorial on support vector regression," *Statist. Comput.*, vol. 14, pp. 199–222, Aug. 2004.

[48] M. L. Stein, *Interpolation of Spatial Data: Some Theory for Kriging*. Springer, 2012.

[49] J. D. Jakeman, A. Narayan, and T. Zhou, "A generalized sampling and preconditioning scheme for sparse approximation of polynomial chaos expansions," *SIAM J. Sci. Comput.*, vol. 39, no. 3, pp. A1114–A1144, Jan. 2017.

[50] C.-C. Chang and C.-J. Lin, "LIBSVM: A library for support vector machines," *ACM Trans. Intell. Syst. Technol.*, vol. 2, no. 3, p. 27, 2011.

[51] C. Cortes and V. Vapnik, "Support-vector networks," *Mach. Learn.*, vol. 20, pp. 273–297, Sep. 1995.

[52] B. Baesens, S. Viaene, T. Van Gestel, J. Suykens, G. Dedene, B. De Moor, and J. Vanthienen, "Least squares support vector machine classifiers: An empirical evaluation," Dept. Toegepaste Economische Wetenschappen, Appl. Econ. Sci., Katholieke Univ. Leuven, Leuven, Belgium, DTEW Res. Rep. 0003, 2000, pp. 1–16.

[53] D. Xiu and G. E. Karniadakis, "The wiener-askey polynomial chaos for stochastic differential equations," *SIAM J. Sci. Comput.*, vol. 24, no. 2, pp. 619–644, Jan. 2002.

[54] Z.-H. Wang, D.-Y. Gong, X. Li, G.-T. Li, and D.-H. Zhang, "Prediction of bending force in the hot strip rolling process using artificial neural network and genetic algorithm (ANN-GA)," *Int. J. Adv. Manuf. Technol.*, vol. 93, nos. 9–12, pp. 3325–3338, Dec. 2017.

[55] X. Tang, L. Zhuang, J. Cai, and C. Li, "Multi-fault classification based on support vector machine trained by chaos particle swarm optimization," *Knowl.-Based Syst.*, vol. 23, no. 5, pp. 486–490, Jul. 2010.

[56] L. Xu, X. Du, and B. Wang, "Short-term traffic flow prediction model of wavelet neural network based on mind evolutionary algorithm," *Int. J. Pattern Recognit. Artif. Intell.*, vol. 32, no. 12, Dec. 2018, Art. no. 1850041.

[57] S. Chengyi, X. Keming, C. Mingqi, "Mind evolution based machine learning framework and new development," *J. Taiyuan Univ. Technol.*, vol. 30, no. 5, pp. 453–457, 1999. Accessed: Dec. 20, 2019. [Online]. Available: http://www.cqvip.com/qk/90007a/199905/3768392.html

[58] L. Yanqing and D. Yingying, "Short-term photovoltaic power forecasting based on optimal similarity and radial basis function neural networks optimized by improved mind evolutionary algorithm," *J. North China Electr. Power Univ.*, vol. 45, pp. 29–36, 2018, doi: 10.3969/j.ISSN.1007-2691.2018.05.04.

[59] F. Pianosi and T. Wagener, "A simple and efficient method for global sensitivity analysis based on cumulative distribution functions," *Environ. Model. Softw.*, vol. 67, pp. 1–11, May 2015, doi: 10.1016/j.envsoft.2015.01.004.

[60] E. Borgonovo, "Measuring uncertainty importance: Investigation and comparison of alternative approaches," *Risk Anal.*, vol. 26, no. 5, pp. 1349–1361, Oct. 2006, doi: 10.1111/j.1539-6924.2006.00806.x.

[61] M. Pedram and S. Nazarian, "Thermal modeling, analysis, and management in VLSI circuits: Principles and methods," *Proc. IEEE*, vol. 94, no. 8, pp. 1487–1501, Aug. 2006, doi: 10.1109/JPROC.2006.879797.

[62] A. J. Chipperfield, "The MATLAB genetic algorithm toolbox," in *Proc. IEE Colloq. Appl. Control Techn. Using MATLAB*, London, U.K., 1995, p. 10, doi: 10.1049/ic:19950061.

[63] A. J. Chipperfield, P. J. Fleming, H. Pohlheim, and C. M. Fonseca, "A genetic algorithm toolbox for MATLAB," in *Proc. Int. Conf. Syst. Eng.*, London, U.K., 1994, vol. 6, no. 8, pp. 200–207.

[64] S. Ebbesen, P. Kiwitz, and L. Guzzella, "A generic particle swarm optimization MATLAB function," in *Proc. Amer. Control Conf. (ACC)*, Jun. 2012, pp. 1519–1524, doi: 10.1109/ACC.2012.6314697.

[65] S. Abid, A. Mouelhi, and F. Fnaiech, "Accelerating the multilayer perceptron learning with the davidon fletcher powell algorithm," in *Proc. IEEE Int. Joint Conf. Neural Netw. Proc.*, Jul. 2006, pp. 3389–3394, doi: 10.1109/IJCNN.2006.247340.

YAN XIONG received the B.S. degree in mechanical design, manufacturing and automation from the School of Engineering, Shenyang Agricultural University, China, in 2015. He is currently pursuing the Ph.D. degree in mechanical manufacturing and automation with the Department of Space Robot Engineering, CIOMP, University of Chinese Academy of Sciences, China. His research interests include intelligent control, spacecraft thermal control, reinforcement learning, and application of machine learning in engineering.

LIANG GUO received the B.S. and M.S. degrees from the Harbin Institute of Technology, China, in 2004 and 2006, respectively, and the Ph.D. degree from the Changchun Institute of Optics, Fine Mechanics and Physics, Chinese Academy of Sciences, China, in 2013. He is currently a Professor with the Changchun Institute of Optics, Fine Mechanics and Physics, Chinese Academy of Sciences. His current research interests include spacecraft thermal control, thermal design, space robot, and intelligent thermal control.

DEFU TIAN received the bachelor's degree in mechanical design, manufacturing and automation from the Changchun University of Technology, China, in 2018. He is currently pursuing the master's degree in mechanical manufacturing and automation with the Department of Space Robot Engineering, CIOMP, University of Chinese Academy of Sciences, China. His research interests include space thermal analysis and heat conduction optimization.

YANG ZHANG received the B.S. degree in mechanical design, manufacturing and automation from the School of Mechanical Engineering and Automation, Northeastern University at Shenyang, Shenyang, China, in 2017. He is currently pursuing the Ph.D. degree in mechanical manufacturing and automation with the Department of Space Robot Engineering, CIOMP, University of Chinese Academy of Sciences, China. His current research interests include parallel mechanism, kinematics, dynamics, and the control of robots.

CHUNLONG LIU received the B.S. and M.S. degrees from the Harbin Institute of Technology, China, in 2007 and 2009, respectively, and the Ph.D. degree, in 2013. He is currently an Associate Professor with the Changchun Institute of Optics, Fine Mechanics and Physics, Chinese Academy of Sciences, China. His current research interests include spacecraft thermal control, engineering thermophysics, and pulverized coal combustion.